

**Phase diagram of oxygen adsorbed on platinum (111) by first-principles investigation**Hairong Tang,<sup>1</sup> Anton Van der Ven,<sup>2</sup> and Bernhardt L. Trout<sup>1,\*</sup><sup>1</sup>*Department of Chemical Engineering, Massachusetts Institute of Technology, 77 Massachusetts Avenue, Cambridge, Massachusetts 02139, USA*<sup>2</sup>*Department of Materials Science and Engineering, Massachusetts Institute of Technology, 77 Massachusetts Avenue, Cambridge, Massachusetts 02139, USA*

(Received 13 November 2003; revised manuscript received 17 February 2004; published 28 July 2004)

A complete phase diagram of oxygen atoms adsorbed on a Pt(111) surface with oxygen coverages below half a monolayer has been computed and compared with the surface phase diagrams of related systems. Effective interaction parameters of a lattice model for the triangular lattice of the fcc sites of the Pt(111) surface were determined from first-principles computations. Oxygen forms on the platinum (111) surface two stable ordered phases, which persist up to high temperatures. They are the  $p(2 \times 2)$  and  $p(2 \times 1)$  phases, having coverages of 1/4 and 1/2 monolayer, respectively. At the coverage of 2/5 monolayer, another stable phase consisting of  $p(2 \times 1)$  rows but with every two rows offset by an empty site is predicted by our model, but this phase is stable only below 250 K. All three phases undergo continuous phase transitions to the disordered state upon heating. At coverages lower than 1/4 monolayer and at low temperatures, oxygen atoms cluster into  $p(2 \times 2)$  islands, in agreement with observations from a scanning tunneling microscope study. The formation of  $p(2 \times 2)$  oxygen islands is a consequence of attractive third-nearest-neighbor interactions, despite the strong repulsion between the first and second nearest neighbors. Two regions separated by first-order phase boundaries are found at coverages between 0.26 monolayer and 0.37 monolayer and coverages between 0.43 monolayer and 0.5 monolayer.

DOI: 10.1103/PhysRevB.70.045420

PACS number(s): 68.43.De, 64.60.Cn, 68.43.Fg, 68.47.De

**I. INTRODUCTION**

Ordering of adsorbates on surfaces is a fairly universal phenomenon at moderate temperatures.<sup>1</sup> Knowledge of the stability of different ordered structures is important for understanding reactions, since reaction rates will be different when the reactants are condensed into different phases. Therefore, a thorough study of the phase diagrams of adsorbates on surfaces is of great importance in describing the thermodynamics and kinetics of processes on surfaces, including adsorption, desorption, diffusion, and chemical reactions.

Oxygen adsorption on metal surfaces, especially on platinum surfaces, has been extensively studied in recent years,<sup>2-5</sup> because of its key role in various important catalytic reactions, such as the three-way and lean-NO<sub>x</sub> automobile catalysts, the manufacture of sulfuric acid, and a variety of other processes involving the oxidation of CO and other chemical species.<sup>6-9</sup> It was found that upon adsorption of oxygen, atomic oxygen is the only species present on platinum surfaces at all but low temperatures<sup>4</sup>. The fcc site, which is the hollow adsorption site without a second-layer metal atom directly beneath the hollow, is found to be the most stable adsorption site of an oxygen atom on Pt(111).<sup>3,8</sup> It was further observed by scanning tunneling microscope (STM) experiments that at submonolayer coverages, small oxygen islands of  $p(2 \times 2)$  symmetry form and merge on a Pt(111) surface, leaving large surface areas of platinum unoccupied.<sup>4</sup> It would be interesting to know why islands of O form. This is a fundamental question for similar, well-organized oxygen islands on other metal surfaces as well, and a thorough understanding of the formation mechanism and phase diagram

of these islands can also be very valuable in determining the mechanisms of important catalytic reactions and processes. Although many studies of the adsorption of atomic oxygen on metal surfaces have been performed before, to our knowledge, only a few phase diagrams of oxygen on metal surfaces have been reported previously. These include O/Ni(111),<sup>10,11</sup> O/Rh(100),<sup>12</sup> O/Ru(0001),<sup>13-15</sup> O/W(110),<sup>16,17</sup> and O/Ni(100).<sup>18,19</sup> No study of the phase diagram of O/Pt has been reported so far. In this paper, we present a phase diagram of the O/Pt(111) surface, computed from first-principles, and compare it with the phase diagrams of other systems.

The symmetry of ordered structures on surfaces is dictated by the interactions between the adsorbates. Thus, having a set of accurate lateral interaction parameters is invaluable for understanding the phase transitions on surfaces. In recent decades, quantitative experimental methods of surface science such as (STM) (Refs. 20 and 21) and low-energy-electron diffraction (LEED) (Ref. 11) have been widely used to evaluate the lateral interactions. On the other hand, first-principles computations<sup>22,23</sup> have also been used in some systems to evaluate the lateral interactions. Of these methods, only first-principles computations can allow one to determine unambiguously the magnitude of various lateral interactions, and this approach was therefore used to determine the various lateral interactions in this study. The lateral interaction parameters extrapolated from the first-principles energies were then used in grand canonical Monte Carlo (GCMC) simulations in order to calculate the phase diagram. Details about the steps used to obtain the phase diagram are described in the next section (Sec. II). Then, in the Sec. III, the results are presented and discussed.

## II. COMPUTATIONAL METHODS

### A. Density functional theory for total energies

First-principles density functional theory (DFT), as implemented in the GNU publicly licensed software DACAPO,<sup>24</sup> was used to compute the total energies. The configuration set selected for the DFT computations was based on seven basic unit cells, as illustrated in Fig. 1. Since the energy of adsorption of oxygen atoms on the fcc sites on Pt(111) is much larger than that on the hcp sites of Pt(111),<sup>3,8</sup> only the fcc sites for O adsorbed on Pt(111) were treated explicitly in this study. Full coverage, also referred to as one monolayer (1 ML), is defined by all the fcc sites on the Pt(111) surface being occupied by oxygen atoms. The largest unit cell chosen in Fig. 1 is a  $(3 \times 3)$  structure. In this cell, the largest O-O separation is equal to three Pt lattice constants and corresponds to the fifth-nearest-neighbor distance of like sites. At these distances, the lateral interactions can be assumed to be negligible.<sup>22</sup> The chemisorption energy of an oxygen atom at the fcc site on Pt(111) on a  $(2 \times 2)$  unit cell with three layers was found to be 4.43 eV, which is in good agreement with the results of other theoretical studies.<sup>9,25</sup> A four-layer slab model with only the bottom layer fixed was also used to check the effects of the finite thickness of the slab model for the Pt $(2 \times 2)$ -O configuration by comparing the formation energy of oxygen to that on the three-layer model. The difference in formation energy between these two slab model calculations is only 0.3 meV. Note that Bogicevic *et al.* have found that the energy change between a four-layer model (with the top two layers fixed) and a six-layer model (with the top four layers fixed) is less than 10 meV.<sup>3</sup> A three-layer Pt model has also been applied by Lynch and Hu in their study of CO and atomic oxygen chemisorption on Pt(111).<sup>8</sup> Therefore, three-layer slab models were used for the Pt(111) surface throughout this study. All the layers were relaxed during optimization except for the bottom layer, which was fixed at the calculated Pt bulk lattice constant 4.00 Å. [This value is close to the experimental value, 3.92 Å (Refs. 26 and 27)]. A vacuum of  $\sim 10$  Å was used to separate the slabs. Between these slabs, we included a point dipole in the Z direction (the direction perpendicular to the slabs) in order to eliminate the interactions among periodic images. The gradient-corrected exchange-correlation functional PW91-GGA (Ref. 28) was used in this study, in addition to ultrasoft pseudopotentials<sup>29,30</sup> and plane-wave expansions with energy cutoffs of 25 Ry (340 eV). The geometry optimization for Pt $(3 \times 3)$ -O was sampled at  $4 \times 4 \times 1$  Monkhorst-Pack  $k$  points.<sup>31</sup> In order to have the same precision, a larger number of  $k$  points corresponding to a larger surface Brillouin zone were used for smaller systems. In order to determine the importance of spin polarization in the O/Pt(111) system, spin-polarization calculations were performed on several configurations. We found that spin polarization usually lowers the formation energy by about 1.5 meV, which is well within the numerical accuracy of the pseudopotential methods. All total-energy calculations in this study were therefore nonmagnetic. The accuracy of all the models and parameters used here have been tested and confirmed in previous studies in our laboratory.<sup>7,32,33</sup>

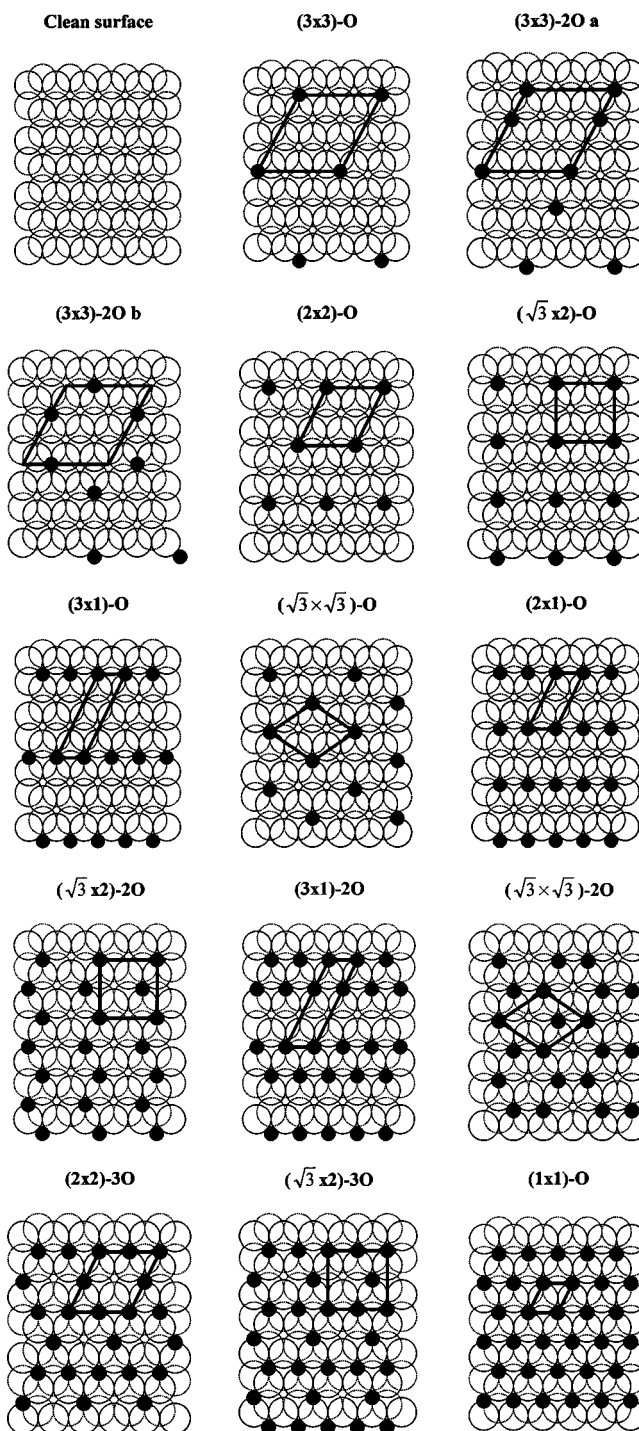


FIG. 1. Adsorbed oxygen configurations calculated using DFT-GGA computations. Large open circles represent Pt atoms and small solid circles represent O atoms. Unit cells are marked in each configuration.

### B. Cluster expansion for lateral interaction parameters

Lateral interactions were modeled via cluster expansions, and the parameters in the cluster expansions were obtained from a small number of first-principles calculations. The energy of any configuration could then be computed using a cluster expansion. A detailed description of the cluster ex-

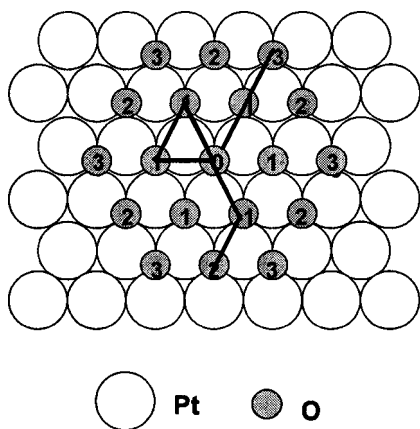


FIG. 2. Lateral interactions between and among oxygen atoms adsorbed on Pt (111). Small circles represent oxygen atoms and large circles represent platinum atoms.

pansion methods and the effect of truncating the expansion can be found in a previous paper.<sup>34</sup> Here we will only give a brief summary of the cluster expansion used in this work.

In order to specify a configuration, a site occupation variable is assigned to each adsorption site on the surface. Any configuration is then represented by a vector composed of all the site occupation variables. Different choices of the site occupation variables are possible and two sets of the site operators have been used in our study.

Each element in the first set of site occupation variables,  $\{\sigma_i\}$ , takes the value +1 if the site is occupied and -1 if a vacancy is at that site. These site occupation variables are also called spin variables, due to their correspondence with the Ising model.<sup>35</sup> It has been shown that the dependence of any property of a configuration can be expanded exactly in terms of polynomials consisting of products of discrete site occupation variables  $\sigma_i$ , where  $\sigma_i = \pm 1$ .<sup>36</sup> For computational convenience, these occupation variables were used in the Monte Carlo simulations in our studies. A cluster expansion of the energy, with the assumption that oxygen only adsorbs on the fcc site on Pt (111), then takes the following form:

$$E(\sigma) = V_0 + \sum_i V_i \sigma_i + \sum_{i,j} V_{i,j} \sigma_i \sigma_j + \sum_{i,j,k} V_{i,j,k} \sigma_i \sigma_j \sigma_k + \dots, \quad (1)$$

where all the coefficients ( $V$ 's) are called effective cluster interactions (ECI's). The interactions up to third nearest neighbors are illustrated in Fig. 2, in which the oxygen atoms marked 1 are the first-nearest-neighbor atoms to the oxygen atom marked 0. Similarly, those marked 2 and 3 are the second and third nearest neighbors to the oxygen atom 0. Here  $v_{i,j}$  and  $v_{i,j,k}$  are pair and three-body interactions, respectively. Treating interactions up to three bodies and third nearest neighbors was found in our previous study to be sufficient to model the system with a high degree of accuracy.<sup>34</sup> With the truncation, the ECI's were fit to first-principles energies of different oxygen-vacancy arrangements (Fig. 1) and were then used to calculate the formation energy of any configuration.

A second set of site operators is also used, as these enable a more physical interpretation of the results. The occupation variables of this set,  $P_i$ , have the value 0 when site  $i$  is vacant and the value +1 when the site is occupied. It is also called a point variable.<sup>37</sup> In the case of only one adsorbed species (oxygen atoms) in the system, we can write the configurational energy of adsorbed oxygen on fcc sites of Pt (111) as

$$E(P) = W_0 + \sum_i W_i P_i + \sum_{i,j} W_{i,j} P_i P_j + \sum_{i,j,k} W_{i,j,k} P_i P_j P_k + \dots, \quad (2)$$

where  $P_i = 1$  (occupied) and 0 (vacant), and where the  $W$ 's are similar to the  $V$ 's of Eq. (1). Here  $W$  and  $V$  can be related mathematically by using the relationship between  $P_i$  and  $\sigma_i$ :

$$P_i = \frac{1}{2}(1 + \sigma_i). \quad (3)$$

Details can be found in Inden and Pitsch paper.<sup>38</sup> It is worth pointing out that only the  $W$ 's in Eq. (2) can be associated with the interactions between oxygen atoms on the surface illustrated in Fig. 2. Within this representation, we set the interactions between oxygen and vacancies and between vacancies and vacancies equal to zero. Thus, interactions represented by  $W$ 's will be used to discuss and explain island formation on the Pt surface in Sec. III B.

### C. Monte Carlo simulations

As mentioned in Sec. II B, lateral interactions  $V_{i,j}$ ,  $V_{i,j,k}$  between oxygen atoms on the Pt (111) surface for the first set of site operators were used in grand canonical Monte Carlo simulations to compute the phase diagram of O/Pt(111). The Monte Carlo simulations were typically performed on a  $30 \times 30$  two-dimensional lattice with periodic boundary conditions, which has been shown to be sufficient for the O/W(110) system.<sup>17</sup> A lattice with the size  $60 \times 60$  was used to check the finite-size effect on our Monte Carlo results. We found that a  $30 \times 30$  two-dimensional (2D) lattice is sufficient to simulate the surface phase diagram of the O/Pt(111) system in this study. Here 2000 Monte Carlo passes per lattice site were performed for equilibration, followed by 5000 Monte Carlo passes per site for sampling at each temperature ( $T$ ) and chemical potential ( $\mu$ ). The continuous phase transition boundaries between the ordered phase and disordered phase were determined by connecting the positions at which the heat capacity or susceptibility diverged at various chemical potentials. At first-order phase transitions (in the grand-canonical ensemble), bulk properties such as the grand-canonical energy or the coverage (oxygen concentration) are discontinuous. However, the occurrence of hysteresis in numerical simulations at first-order phase transitions makes a precise determination of their location difficult. A reliable way of determining first-order phase boundaries is with the common tangent construction applied to constant temperature Gibbs free energy curves of the two phases participating in the transition. (This is equivalent to determining the location at which the grand-canonical free energies of the two phases competing for stability cross.) In a composition versus temperature phase diagram, first-order phase transitions

TABLE I. Formation energies (in meV) for O on Pt (111) for various coverages (all of the configurations can be found in Fig. 1).

Label	Configuration	Coverage of O (ML)	Formation energy (meV)
a	Clean Pt (111) surface	0	0.000
b	(3×3)-O	1/9	-107.670
c	(3×3)-2O <sup>a</sup>	2/9	-189.641
d	(3×3)-2O <sup>b</sup>	2/9	-202.428
e	(2×2)-O	1/4	-245.525
f	(√3×2)-O	1/4	-229.897
g	(3×1)-O	1/3	-233.265
h	(√3×√3)-O	1/3	-283.512
i	(2×1)-O	1/2	-340.318
j	(√3×2)-2O	1/2	-326.729
k	(3×1)-2O	2/3	-266.384
l	(√3×√3)-2O	2/3	-318.790
m	(2×2)-3O	3/4	-261.702
n	(√3×2)-3O	3/4	-260.625
o	(1×1)-O	1	0.000

at constant temperature appear as two phase coexistence regions. For any composition inside the two phase region, the thermodynamically stable state consists of two coexisting phases. We obtained Gibbs free energy curves at constant temperature by integrating the chemical potential versus composition from suitable reference states.<sup>23,39</sup>

At very low temperatures, the flipping probability becomes very small, and virtually nothing happens for a long time. Therefore, an event-driven algorithm (the  $N$ -fold way Ref. 40) was used for the Monte Carlo simulations at temperatures below 300 K. The  $N$ -fold way algorithm is similar to the kinetic Monte Carlo algorithm but without physically relevant rate constants: a list of all the events with their probabilities is built and updated during each step of the simulation, and a flip, determined by a random number, occurs at each step. At low temperatures, the net gain in performance of the  $N$ -fold way algorithm is dramatic, although each flip takes a considerable amount of CPU time.

### III. RESULTS AND DISCUSSIONS

#### A. Formation energies of oxygen adsorbed on Pt (111)

For purposes of understanding phase stability, it is often convenient to consider formation energies instead of adsorption energies. The formation energy of a particular configuration at a given coverage ( $\theta$ ) of oxygen on Pt (111) is defined as

$$\Delta_f E = E_{O-Pt} - (1 - \theta)E_{Pt} - \theta E_{P(1 \times 1)-O}, \quad (4)$$

where  $E_{O-Pt}$  is the total energy for a configuration of oxygen atoms adsorbed on Pt (111) with the coverage  $\theta$ ,  $E_{Pt}$  is the total energy for a clean Pt (111) surface, and  $E_{P(1 \times 1)-O}$  is the total energy of oxygen adsorbed on Pt (111) at full coverage. The formation energy clearly illustrates the stability of the ordered oxygen configurations relative to a mixture of a

clean surface and a surface with full coverage of oxygen at the same overall composition.

Formation energies were determined by inserting DFT total energies of 15 configurations (refer to Table I and Fig. 1) of oxygen adsorbed on Pt (111) (with oxygen coverages ranging from 0 to 1) into Eq. (4). As plotted in Fig. 3, the formation energies of all the configurations are negative. In order to analyze phase stability at 0 K, we constructed the convex hull of the formation energies, as illustrated by the solid lines in Fig. 3. In general, phase stability is determined by the state with the lowest free energy. In a binary system, the common tangent construction determines phase stability when two phases can simultaneously coexist. At 0 K, the free energy equals the energy and hence the convex hull can be viewed as a set of common tangents connecting the energies of the most stable phases. At any composition between two stable phases connected by a line of the convex hull, the thermodynamically most stable state consists of a phase separation of those two phases. Typically the phases on the convex hull remain stable as the temperature is increased, though phases that are marginally stable tend to disorder at

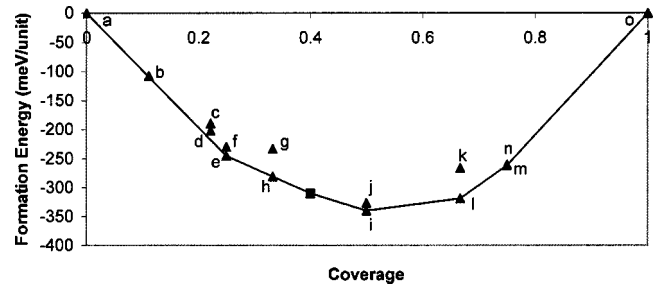

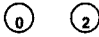

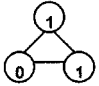

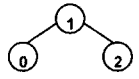


FIG. 3. Formation energies of adsorbed oxygen atoms on Pt (111) (the square point was not included in the fitting of the lateral interaction parameters, but was used as a test for our cluster expansion). Labels (a)–(o) correspond to those in Table I.

TABLE II. Fitted ECI's by using a cluster expansion with the first set of site operators for O/Pt (111).

ECI's		meV
	$V_{01}$	72.367
	$V_{02}$	12.345
	$V_{03}$	2.936
	$V_{011}$	-0.684
	$V_{013}$	4.664
	$V_{012}$	1.501

low temperatures and may not appear at reasonable temperatures in a temperature composition phase diagram. We find that of the original 12 configurations considered, 5 appear on the convex hull. These stable phases are  $p(2 \times 2)$ -O, with a coverage of  $1/4$  ML,  $p(\sqrt{3} \times \sqrt{3})$ -O, with a coverage of  $1/3$  ML,  $p(2 \times 1)$ -O, with a coverage of  $1/2$  ML,  $p(\sqrt{3} \times \sqrt{3})$ -2O, with a coverage of  $2/3$  ML, and  $p(2 \times 2)$ -3O, with a coverage of  $3/4$  ML. While the configuration  $p(3 \times 3)$ -O has a formation energy close to the convex hull, it does not lie on the convex hull and, hence, cannot be expected to be present in a temperature composition phase diagram. At the end of this section, we will show that  $p(2 \times 2)$ -O and  $p(2 \times 1)$ -O remain stable up to reasonably high temperatures.

### B. Lateral interaction parameters




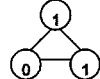

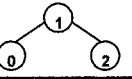
The fitted interaction parameters for both sets of site operators described in Sec. II B are listed in Table II (spin variable set) and Table III (point variable set). As mentioned in the previous cluster expansion part, the spin variable set is convenient for computational purposes, while the point variable set offers a more physical interpretation of the interactions. By using the mathematical relationship between the two sets of site operators, Eq. (3), the lateral interactions  $W_{i,j}$  for cluster expansion with the point variable set can be written as linear combinations of the  $V_{i,j}$  corresponding to the spin variable set. The interaction parameters  $V_{i,j}$  and  $W_{i,j}$  have been shown to be consistent with each other in a previous study.<sup>34</sup>

As shown in Table III, the repulsion between the nearest neighbor oxygen atoms on Pt (111) is about 0.24 eV. Lynch and Hu used the DFT and generalized gradient approximation (GGA) computation and found that the energy difference between oxygen adsorption at fcc and hcp sites on

Pt (111) is 0.47 eV.<sup>8</sup> Therefore, in the O/Pt(111) system, the binding energy difference of an oxygen atom between fcc and hcp sites is much higher than the nearest-neighbor repulsive interactions between adsorbed oxygen atoms on the Pt (111) surface. This result is consistent with our assumption that the occupation of hcp sites is not very important in determining the phase diagram of O/Pt(111). It is also different from the O/Ru(0001) system, in which the hcp site is preferred over the fcc site by 0.072 eV at the DFT-GGA level of theory, much less than the first-nearest-neighbor repulsion between oxygen atoms on hcp sites (0.27 eV).<sup>22</sup>

We emphasized in Sec. II B that a straightforward physical interpretation can not be assigned to the interaction parameters  $V_{i,j}$  of Eq. (1), but  $W_{i,j}$ , the coefficients of Eq. (2), can be physically interpreted. They are effective interactions among atoms on a Pt (111) surface. In Table III, the lateral interaction parameters  $W_{i,j}$  indicate that there exists a strong repulsion between nearest-neighbor oxygen atoms (0.237 eV), relatively strong repulsions between next nearest-neighbor oxygen atoms (0.040 eV), and a weak attraction between third nearest neighbors (-0.006 eV). No known experimental energies of interactions for O/Pt(111) are available for comparison with our results here, but we can compare our results with those for O/Ru(0001), both of which have triangular lattices in which adsorption occurs at well-defined sites [fcc for O/Pt(111) and hcp for O/Ru(0001)]. The interactions determined by Piercy *et al.* for their best fit to the experimental O/Ru (0001) phase diagram<sup>14</sup> are given in brackets in Table III. The interactions derived by Stampfl *et al.* for O/Ru(0001) from first-principles calculations<sup>22</sup> are given in parenthesis in Table III. It is found that the pairwise interactions that we obtained for O/Pt(111) are similar to both the experimental and theoretical interactions for O/Ru(0001).

TABLE III. Fitted ECI's by using a cluster expansion with the second set of site operators for O/Pt(111). In brackets, we list the interaction parameters fitted by Piercy *et al.* from the experimental O/Ru(0001) phase diagram (Ref. 14). In parentheses, we list the interaction parameters derived by Stampfl *et al.* from DFT computations for O/Ru(0001) (Ref. 22).

ECI's		meV		
	$W_{01}$	237.088	[230]	(265)
	$W_{02}$	39.498	[69]	(44)
	$W_{03}$	-5.808	[-23]	(-25)
	$W_{011}$	12.914		
	$W_{013}$	29.567		
	$W_{012}$	6.302		

The repulsions between the nearest- and next-nearest-neighbor oxygen atoms on Pt(111) can be explained by bond-competition concepts, which have been applied to other systems previously.<sup>8,9,41,42</sup> The effects of the adsorbed oxygen atoms on the projected density of states (pDOS) of their neighbor Pt atoms are illustrated in Fig. 4. The order of effects induced by the adsorbed oxygen atom to its neighbor Pt atoms is the following: nearest Pt neighbors  $\gg$  next nearest Pt neighbors  $>$  third nearest Pt neighbors. According to the bond-competition concept, if coadsorbed atoms have to compete with each other for bonding with the surface metal atoms, it would be expected that the most stable adsorption configuration involves the minimum possible amount of competition. Since the adsorbed oxygen atoms have a strong and reasonably strong effect on their first- and second-

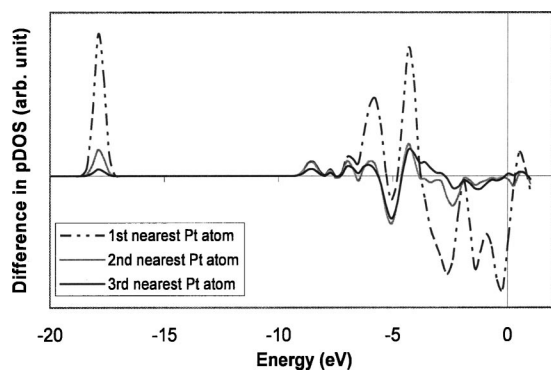


FIG. 4. Comparison among the changes of projected density of states (pDOS) of Pt atoms at different distances from an adsorbed oxygen atom. (The differences are with respect to Pt atoms of the same symmetry at clean surfaces.)

nearest-neighbor Pt atoms, respectively, any coadsorbed oxygen atoms which compete for bonding with the same Pt atoms should suffer an energetic penalty to adsorb, due to the repulsions to the already adsorbed oxygen atoms. On the other hand, Table III clearly shows an attraction between third nearest neighbors. We explain this using an argument similar to that of Feibelman, who studied O adsorbed on Pt(111).<sup>43</sup> He showed that when an oxygen atom (oxygen *a* in Fig. 5) is adsorbed on an fcc site on Pt(111), the *d* electrons of its Pt nearest neighbors (Pt 1*a*, 1*b*, and 2*a* in Fig. 5) are “frustrated” by two incompatible demands. The first is to get as far away from the negatively charged O atom as possible. The other one is to avoid weakening Pt-Pt bonds by filling antibonding *d* states. These two demands together strengthen the bond between Pt atoms 1*a* and 2*c* and the bond between Pt atoms 1*b* and 2*b* (refer to Fig. 5). Therefore, the overall adsorption of the oxygen atom is strengthened. Similarly, in Fig. 5, the bond between Pt atoms 1*c* and 2*c* and the bond between Pt atoms 1*d* and 2*b* are both

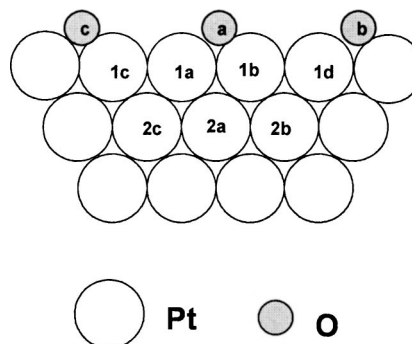


FIG. 5. Side view of configuration  $p(2 \times 2)$ -O.

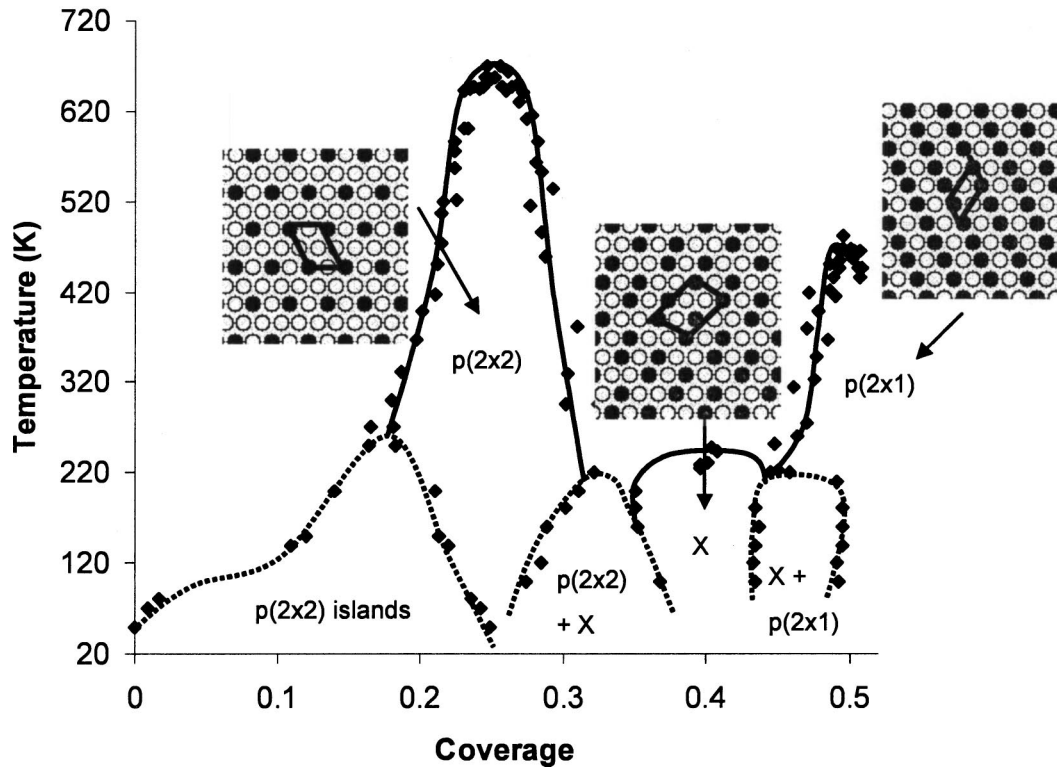


FIG. 6. Phase diagram of O/Pt(111): the solid lines denote continuous phase transitions and the dotted lines denote first-order phase transitions.

strengthened. It turns out that these strengthening of bonds is optimized for  $p(2 \times 2)$ .

### C. Phase diagram of O/Pt(111)

The calculated equilibrium phase diagram of O/Pt(111) with oxygen coverages of up to half a monolayer is presented in Fig. 6, where the solid lines are continuous phase transition boundaries and the dashed lines signify the boundaries of two-phase coexistence regions (first-order phase transitions). It can be seen that chemisorption of oxygen atoms on Pt (111) leads to two ordered phases at temperatures between about 200 K and 700 K. They are the  $p(2 \times 2)$  phase, with an oxygen coverage of 1/4 ML, and the  $p(2 \times 1)$  phase, with an oxygen coverage of 1/2 ML. The corresponding configurations are shown in the insets in Fig. 6. The presence of the two phases is similar to results in the literature for O/Ru(0001).<sup>14,22</sup> Also, similar to the experimental and theoretical results of O/Ru(0001),<sup>14</sup> the boundaries of both the  $p(2 \times 2)$  and the  $p(2 \times 1)$  phases in our O/Pt(111) phase diagram denote continuous phase transitions. The order-disorder transition temperatures for the stoichiometric  $p(2 \times 2)$  phase and  $p(2 \times 1)$  phase are predicted to be 670 K and 480 K, respectively. We note that automotive catalysts typically run at temperatures greater than 950 K,<sup>44</sup> and we would expect no ordered phases in this region. Kaburagi and Kanamori studied the ordered ground states of the triangular lattice and found that  $p(2 \times 2)$ -O can be stabilized if  $V_{01} > 5V_{02} > 0$  which is exactly the case in our system (refer to Table II).<sup>45,46</sup>

At finite temperature, defects and antiphase boundaries can occur, and due to the symmetry of  $p(2 \times 1)$ , domains having rows with different directions, which are rotated by  $120^\circ$  with respect to each other, can coexist (see the zigzag structure in Fig. 7). Similar behavior has also been observed in the STM study of other systems, such as the O/Ru(0001) system by Meinel *et al.*<sup>2</sup> and the Au (111) system by Barth *et al.*,<sup>47</sup> but these were thought to be caused by a long-range elastic lattice strain.<sup>48</sup> We attribute our zigzag structure to sluggish “kinetics” in Monte Carlo simulations.

Our phase diagram for O/Pt(111) is quite different from the O/Ni(111) phase diagram measured by Kortan and Park.<sup>10</sup> Although both systems show  $p(2 \times 2)$  phases at a coverage of around 1/4 ML, unlike the O/Ni(111) phase diagram, our O/Pt(111) phase diagram contains no stable phase with a coverage of 1/3 ML — e.g., a  $p(\sqrt{3} \times \sqrt{3})$ -O phase at intermediate to high temperatures. Note that the  $p(\sqrt{3} \times \sqrt{3})$ -O ordered phase is marginally stable at 0 K (i.e., it is on the convex hull), and therefore it should be observed at sufficiently low temperatures. At a low temperature and when the coverage equals 2/5 ML, a small phase with a continuous transition boundary appears in our phase diagram. The order-disorder transition temperature of this phase is about 250 K. In this phase, every two  $p(2 \times 1)$  oxygen rows are offset by an empty site (see the inset between those for  $p(2 \times 2)$  and  $p(2 \times 1)$  phases in Fig. 6). In other words, it is characterized by a unit cell which is a combination of  $p(\sqrt{3} \times \sqrt{3})$  and  $p(2 \times 1)$ . Since it is hard to name it in a conventional way, we denote this phase region X in Fig. 6. Note that we found that the cluster expansion used to calcu-

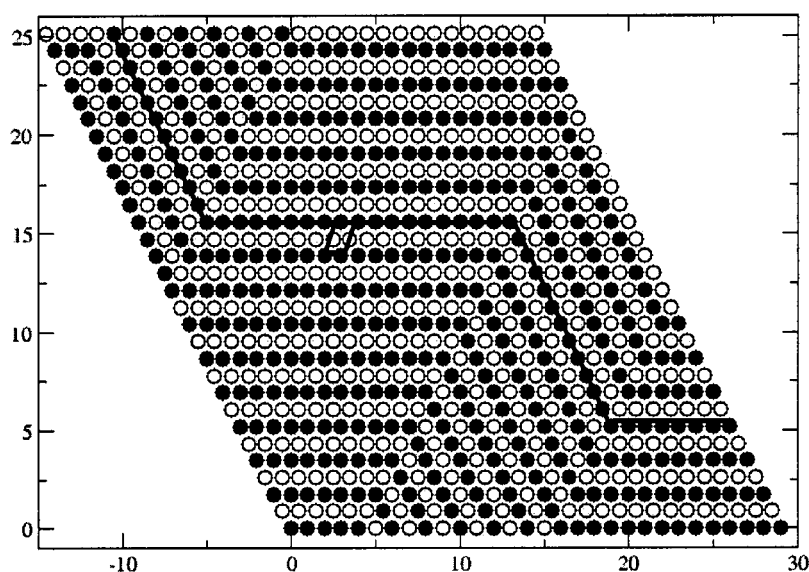


FIG. 7. A sample configuration of the ordered oxygen phase having the symmetry  $p(2 \times 1)$  on Pt (111) with  $p(2 \times 1)$  rows rotated by  $120^\circ$  with respect to each other.

late the phase diagram predicts the  $X$  phase to be on the convex hull. Furthermore, clear thermodynamic discontinuities were observed in the Monte Carlo simulations when crossing from the  $X$  phase to the disordered phase or to the  $p(2 \times 2)$  or  $p(2 \times 1)$  phases. Hence the  $X$  phase is a distinct stable phase. Phase  $X$  is an unexpected phase from our original formation energy curve, since we did not include any DFT energy for a configuration at an oxygen coverage equaling to  $2/5$  ML in the fit of the cluster expansion. To prove that phase  $X$  is a stable phase on the 2D lattice, we performed a DFT computation with the same unit cell as marked in the inset configuration corresponding to the phase  $X$  in Fig. 6. The formation energy of the new configuration, marked as a square in Fig. 3, does appear on the convex hull. This not only proves that the new configuration is a stable phase, but also shows that our cluster expansion is robust enough to predict the energies for configurations that were not included in the fit of the interaction parameters. Experimental effort around an oxygen coverage of 0.4 ML is suggested in order to confirm the DFT prediction of the stability of phase  $X$ .

In our O/Pt(111) phase diagram, there are three regions separated by first-order phase boundaries, which means that those regions are two-phase coexistent regions. The first one appears at low temperatures and low coverages, where a first-order phase transition occurs from the  $p(2 \times 2)$  phase to the disordered lattice gas phase. The coexistent region is therefore characterized by a state with  $p(2 \times 2)$  islands. A typical  $p(2 \times 2)$  oxygen island configuration obtained from Monte Carlo simulations at 100 K with a coverage of 0.09 ML is illustrated in Fig. 8. At 100 K, when the oxygen atoms adsorb with a coverage of 0.09 ML,  $p(2 \times 2)$  oxygen islands with different sizes are predicted to form on the Pt (111) surfaces. This is in good agreement with the STM study of Stipe *et al.*, in which it was found that regions of  $p(2 \times 2)$  symmetry began to appear when the Pt (111) surface was dosed at 82 K and then warmed to 156 K (see Fig. 9).<sup>4</sup> In Fig. 9, the island with the mark  $p(2 \times 2)$  includes about 15 oxygen atoms, a size which is similar to those in our simulations. A tricritical point, corresponding to the in-

tersection of boundaries of a  $p(2 \times 2)$  phase region, a disordered phase, and a mixed phase region of  $p(2 \times 2)$  islands surrounded by the disordered phase, was found at the coverage of 0.18 ML, when the temperature is about 270 K. This is similar to the tricritical point ( $T=300$  K,  $\theta=0.21$  ML) in the experimental phase diagram of O/Ni(111).<sup>10</sup> We attribute the further stabilization of  $p(2 \times 2)$  oxygen islands to the attractions between the third nearest neighbors (refer to Table III). Piercy *et al.* compared the phase diagrams calculated via Monte Carlo simulations with and without attractive third-nearest-neighbor interactions. They found that  $p(2 \times 2)$  islands grow at a coverage below  $1/4$  ML at low temperatures when an attractive third-nearest-neighbor pair interaction is included. However,  $p(2 \times 2)$  islands do not form when the phase diagram was simulated without a third-nearest-neighbor attractive pair interaction.<sup>14</sup> We found that as we increase the oxygen chemical potential, the  $p(2 \times 2)$  phase transforms to the  $(2 \times 1)$  phase at low temperatures by first passing through a coexistent region of  $p(2 \times 2)$  and  $X$  at coverages between 0.26 ML and 0.37 ML, followed by a

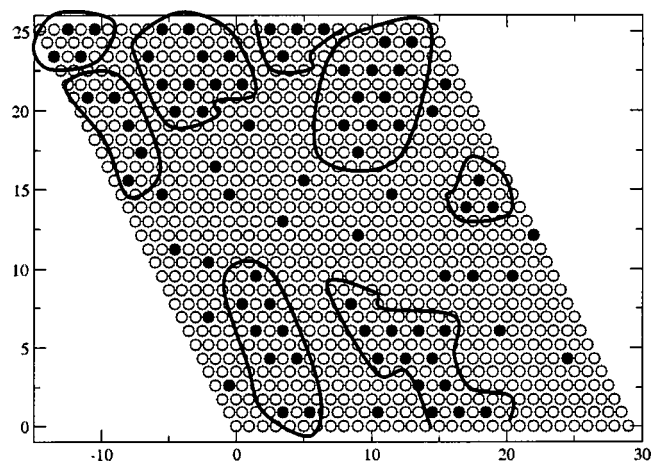


FIG. 8. Regions characterized as  $p(2 \times 2)$  oxygen islands in a snapshot of a GCMC calculation ( $T=100$  K,  $\mu=-979$ , and  $\theta=0.09$  ML).



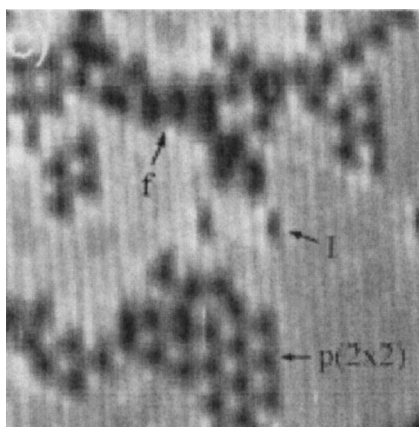


FIG. 9. Oxygen on Pt (111) dosed at 82 K and warmed to 152 K. Bright atoms are Pt and dark atoms are O.  $70 \text{ \AA} \times 70 \text{ \AA}$ . Reproduced with permission from Ref. 4.

single phase region  $X$  around  $2/5$  ML, and then another two-phase region of  $X$  and  $p(2 \times 1)$  at coverages higher than 0.43 ML.

#### IV. CONCLUSIONS

The surface phase diagram of the O/Pt(111) system has been computed from first-principles. This was accomplished by performing grand canonical Monte Carlo simulations on a

2D lattice and incorporating up to next-next-nearest-neighbor interactions that were determined from density functional theory computations. Our results indicate that oxygen atoms adsorbed on Pt (111) form well-ordered  $p(2 \times 2)$  (at  $1/4$  ML) and  $p(2 \times 1)$  (at  $1/2$  ML) phases with continuous phase boundaries. The order-disorder phase transition temperatures of these two phases are 670 K and 480 K, respectively. Oxygen atoms are shown to cluster into  $p(2 \times 2)$  islands at coverages lower than  $1/4$  ML at low temperatures, which is in agreement with the STM experiments of Stipe *et al.* The stabilization of oxygen  $p(2 \times 2)$  islands on Pt (111) is a consequence of the attractive third-nearest-neighbor interactions between the adsorbed oxygen atoms. Other two-phase-coexistent regions are found to exist between coverages of 0.26 ML and 0.37 ML and between coverages of 0.43 ML and 0.5 ML. At temperatures lower than 250 K, a new stable phase at the coverage of  $2/5$  ML consisting of two  $p(2 \times 1)$  rows offset by an empty site was found. This phase has a continuous phase transition boundary, and we designate it phase  $X$ .

#### ACKNOWLEDGMENTS

This work was supported in part by the National Science Foundation, Grant No. CTS-9984301, and by Ford Motor Company. The authors thank Professor Ceder from the Department of Materials Science and Engineering at MIT for his helpful suggestions.

\*Author to whom correspondence should be addressed. Electronic address: trout@mit.edu

<sup>1</sup>R. I. Masel, *Principles of Adsorption and Reaction on Solid Surfaces* (Wiley, New York, 1996), Chap. 4 p. 254.

<sup>2</sup>K. Meinel, H. Wolter, Ch. Ammer, A. Beckmann, and H. Neddermeyer, *J. Phys.: Condens. Matter* **9**, 4611 (1997).

<sup>3</sup>A. Bogicevic, J. Strömquist, and B. I. Lundqvist, *Phys. Rev. B* **57**, R4289 (1998).

<sup>4</sup>B. C. Stipe, M. A. Rezaei, and W. Ho, *J. Chem. Phys.* **107**, 6443 (1997).

<sup>5</sup>J. Wintterlin, R. Schuster, and G. Ertl, *Phys. Rev. Lett.* **77**, 123 (1996).

<sup>6</sup>K. C. Taylor, J. R. Anderson, and M. Boudart, *Catalysis Science and Technology* (Springer-Verlag, New York, 1984), Chap. 5, p. 119.

<sup>7</sup>X. Lin, K. C. Hass, W. F. Schneider, and B. L. Trout, *J. Phys. Chem. B* **106**, 12 575 (2002).

<sup>8</sup>M. Lynch and P. Hu, *Surf. Sci.* **458**, 1 (2000).

<sup>9</sup>K. Bleakley and P. Hu, *J. Am. Chem. Soc.* **121**, 7644 (1999).

<sup>10</sup>A. R. Kortan and R. L. Park, *Phys. Rev. B* **23**, 6340 (1981).

<sup>11</sup>C. Schwennicke and H. Pfnür, *Phys. Rev. B* **56**, 10 558 (1997).

<sup>12</sup>A. Baraldi, V. R. Dhanak, G. Comelli, K. C. Prince, and R. Rosei, *Phys. Rev. B* **56**, 10 511 (1997).

<sup>13</sup>K. De'Bell, H. Pfnür, and P. Piercy, in *The Structure of Surfaces III*, edited by S. Y. Tong (Springer-Verlag, Berlin, 1991), p. 437.

<sup>14</sup>P. Piercy, K. De'Bell, and H. Pfnür, *Phys. Rev. B* **45**, 1869 (1992).

<sup>15</sup>G. Xiong and X. Li, *Commun. Theor. Phys.* **35**, 114 (2001).

<sup>16</sup>G. C. Wang, T. M. Lu, and M. G. Lagally, *J. Chem. Phys.* **69**, 479 (1978).

<sup>17</sup>I. Vattulainen, S. C. Ying, T. Ala-Nissila, and J. Merikoski, *Phys. Rev. B* **59**, 7697 (1999).

<sup>18</sup>D. E. Taylor and R. L. Park, *Surf. Sci.* **125**, L73 (1983).

<sup>19</sup>P. Piercy and H. Pfnür, *Phys. Rev. Lett.* **59**, 1124 (1987).

<sup>20</sup>J. Trost, T. Zambelli, J. Wintterlin, and G. Ertl, *Phys. Rev. B* **54**, 17 850 (1996).

<sup>21</sup>L. Österlund, M. Ø. Pedersen, I. Stensgaard, E. Lægsgaard, and F. Besenbacher, *Phys. Rev. Lett.* **83**, 4812 (1999).

<sup>22</sup>C. Stampfl, H. J. Kreuzer, S. H. Payne, H. Pfnür, and M. Scheffler, *Phys. Rev. Lett.* **83**, 2993 (1999).

<sup>23</sup>A. Van der Ven, M. K. Aydinol, G. Ceder, G. Kresse, and J. Hafner, *Phys. Rev. B* **58**, 2975 (1998).

<sup>24</sup><http://www.fysik.dtu.dk/CAMP/dacapo.html>.

<sup>25</sup>B. Hammer and J. K. Nørskov, in *Chemisorption and reactivity on supported clusters and thin films*, edited by R. M. Lambert, G. Pacchioni (Kluwer Academic, Dordrecht, 1997), p. 285.

<sup>26</sup>C. Kittel, *Introduction to Solid State Physics*, 7th edition (Wiley & Sons, New York, 1996), p. 23.

<sup>27</sup>N. W. Ashcroft and N. D. Mermin, in *Solid State Physics*, edited by D. G. Crane (Harcourt Brace College, Orlando, FL, 1976).

<sup>28</sup>J. P. Perdew, J. A. Chevary, S. H. Vosko, K. A. Jackson, M. R. Pederson, D. J. Singh, and C. Fiolhais, *Phys. Rev. B* **46**, 6671 (1992).

<sup>29</sup>D. Vanderbilt, *Phys. Rev. B* **41**, 7892 (1990).

- <sup>30</sup>K. Laasonen, A. Pasquarello, R. Car, C. Lee, and D. Vanderbilt, Phys. Rev. B **47**, 10 142 (1993).
- <sup>31</sup>H. J. Monkhorst and J. D. Pack, Phys. Rev. B **13**, 5188 (1976).
- <sup>32</sup>X. Lin, N. J. Ramer, A. M. Rappe, K. C. Hass, W. F. Schneider, and B. L. Trout, J. Phys. Chem. B **105**, 7739 (2001).
- <sup>33</sup>X. Lin, W. F. Schneider, and B. L. Trout, J. Phys. Chem. B **108**, 250 (2004).
- <sup>34</sup>H. Tang, A. Van der Ven, and B. L. Trout, Mol. Phys. **102**, 273 (2004).
- <sup>35</sup>P. A. Flinn, Phys. Rev. **104**, 350 (1956).
- <sup>36</sup>J. M. Sanchez, F. Ducastelle, and D. Gratias, Physica A **128**, 334 (1984).
- <sup>37</sup>P. C. Clapp and S. C. Moss, Phys. Rev. **142**, 418 (1966).
- <sup>38</sup>G. Inden and W. Pitsch, in *Materials Science and Technology*, edited by P. Haasen (Verlag Chemie, Weinheim, 1991), Vol. 5, Chap. 9, p. 497.
- <sup>39</sup>A. Van der Walle and M. Asta, Modell. Simul. Mater. Sci. Eng. **10**, 521 (2002).
- <sup>40</sup>D. P. Landau and K. Binder, *A Guide to Monte Carlo Simulations in Statistical Physics* (Cambridge, University Press, Cambridge, England, 2000), Chap. 5, p. 140.
- <sup>41</sup>E. Shustorovich and H. Sellers, Surf. Sci. Rep. **31**, 1 (1998).
- <sup>42</sup>J. Lopez, J. C. Bosse, and J. Rousseau-Violet, J. Phys. C **13**, 1139 (1980).
- <sup>43</sup>P. J. Feibelman, Phys. Rev. B **56**, 10 532 (1997).
- <sup>44</sup>EPA workshop on gasoline sulfur, EPA staff paper on gasoline sulfur issues, Arlington, VA, 1998 (unpublished).
- <sup>45</sup>M. Kaburagi and J. Kanamori, J. Phys. Soc. Jpn. **44**, 718 (1978).
- <sup>46</sup>M. Kaburagi and J. Kanamori, Jpn. J. Appl. Phys., Suppl. **2**, 145 (1974).
- <sup>47</sup>J. V. Barth, H. Brune, G. Ertl, and R. J. Behm, Phys. Rev. B **42**, 9307 (1990).
- <sup>48</sup>F. Besenbacher, Rep. Prog. Phys. **59**, 1737 (1996).